XAFS Spectroscopy Study of Microstructure and Electronic Structure of Heterosystems Containing Si/GeMn Quantum Dots

Erenburg, S. B.; Trubina, S. V.; Zvereva, A.; Zinoviev, A.; Katsyuba, V.; Dvurechenskii, V.; Kvashnina, K. O.; Voelskow, M.;

Originally published:

May 2019

Journal of Experimental and Theoretical Physics 128(2019), 303-311

DOI: https://doi.org/10.1134/S1063776119020067

XAFS Spectroscopy Study of Microstructure and Electronic Structure of Heterosystems Containing Si/GeMn Quantum Dots

S. B. Erenburg[a,b,*], S. V. Trubina[a], V. A. Zvereva[a], V. A. Zinoviev[c], A. V. Katsyuba[c], A. V. Dvurechenskii[c], K. Kvashnina[d,e], and M. Voelskow[f]

[a] *Nikolaev Institute of Inorganic Chemistry, Siberian Branch, Russian Academy of Sciences, Novosibirsk, 630090 Russia*

[b] *Budker Institute of Nuclear Physics, Siberian Branch, Russian Academy of Sciences, Novosibirsk, 630090 Russia*

[c] *Rzhanov Institute of Semiconductor Physics, Siberian Branch, Russian Academy of Sciences, Novosibirsk, 630090 Russia*

[d] *Rossendorf Beamline at the ESRF, Grenoble, 38043 France*

[e] *Helmholtz-Zentrum Dresden-Rossendorf (HZDR), Institute of Resource Ecology, Dresden, 01328 Germany*

[f] *Helmholtz-Zentrum Dresden-Rossendorf (HZDR), Institute of Ion Beam Physics and Materials Research, Dresden, 01328 Germany*

** e-mail: simon@niic.nsc.ru*

Received July 31, 2018; revised September 2, 2018; accepted September 4, 2018

Abstract—Using X-ray absorption near edge structure spectroscopy, extended X-ray absorption fine structure spectroscopy, atomic force microscopy, and Rutherford backscattering spectroscopy, the features of the microstructure and elemental composition of Si/GeMn magnetic systems obtained by molecular beam epitaxy and containing quantum dots are studied. Intense mixing of Ge and Si atoms is found in all samples. The degree of mixing (diffusion) correlates with the conditions of synthesis of Si/GeMn samples. For these systems, direct contacts of germanium atoms with manganese atoms are characterized and the presence of interstitial manganese with tetrahedral coordination and substitution of manganese for germanium and silicon in the lattice sites is found. The presence of stoichiometric phases Ge_8Mn_{11}, Ge_3Mn_5 is not detected. The correlations of the Ge, Si, and Mn coordination numbers in the Ge environment are determined both with the Mn flux value (evaporator temperature) and with the temperature at which quantum dots are grown, as well as with other synthesis conditions. The manganese concentration in the samples is determined.

1. INTRODUCTION

1.1. Ferromagnetic Semiconductors

The discovery of ferromagnetic (FM) semiconductors and the study of their physical properties have long attracted attention of researchers due to their unique magnetic and optical properties and a wide range of possible applications [1–3]. Recently, studies of new FM semiconductors have been carried out, which may enable the use of potential advantages of new functional elements from low power dissipation materials. This possibility can be realized in such systems due to their unique ability to control ferromagnetism by an electric field [4]. Great efforts have already been made along these lines to create and study such new materials. The Ge/Si heterostructures doped with manganese attracted particular attention because of their compatibility with modern silicon microelectronics technology and the possibility of having a higher Curie temperature T_C than temperatures characteristic of $A^{III}B^{V}$ group materials [4].

Recently, great progress has been made in solving fundamental problems of the growth of high-quality germanium films doped with manganese. New manganese-doped germanium structures with controlled ferromagnetism at room temperature are very promising for creating such functional elements as magnetoresistive memory, field sensors, spin transistors, reconfigurable logic devices, and elements for quantum information processing. However, there are problems as well: Experimental results show that manganese is poorly soluble in germanium and prefers to agglomerate to form intermetallic compounds with fairly low FM transition temperatures [4]. Si/GeMn systems containing the layers of quantum dots are very promising for solving these problems [4, 5]. For such structures, the FM behavior at rather high temperatures (above 400 K) and the absence of the stoichiometric Ge_3Mn_5 and Ge_8Mn_{11} phases, which are formed during the synthesis of homogeneous films and have significantly lower FM transition temperatures have been established [4]. Using secondary ion

mass spectrometry (SIMS), it was shown that in Si/GeMn systems containing quantum dots with a 2% manganese content, a GeMn alloy is formed, but in a 10% sample a substantial part of manganese is mixed with silicon to form silicides [5]. Similar Si/GeMn samples with different topology, magnetic impurity content, and preparation conditions were synthesized for our studies by molecular epitaxy.

A promising goal of the research is to determine the optimal composition of the Si/GeMn system that provides the most pronounced magnetic properties.

1.2. EXAFS Spectroscopy for Calculation of Similar Structures

When calculating the energy spectrum of nanosystems and interpreting experimental results related to its features, as well as when designing elements with specified electronic properties, it is necessary to take into account the peculiarities of their local structure. It is known that local distortions of the structure in thin layers and nanoclusters cannot be reliably determined by traditional X-ray diffraction or electron diffraction methods due to the absence of long-range ordering in such systems. Extended X-ray absorption fine structure (EXAFS) and X-ray absorption near edge structure (XANES) spectroscopies using powerful synchrotron radiation sources provide a unique opportunity to solve the problems of this sort [6, 7]. These methods, which are the main in this work, make it possible to determine the parameters of the local environment of atoms: interatomic distances, coordination numbers, symmetry and the type of atoms in the neighborhood, Debye–Waller factors, determine the shifts of electronic levels, and also estimate the charge states of atoms.

It should be noted that recently a number of papers have reported successful applications of EXAFS and XANES to study semiconductor heterosystems containing semiconductor germanium nanoclusters (quantum dots) in silicon [8–15] (including our works [14, 15]), for which the existence of a discrete energy spectrum of charge carriers localized in these systems has been reliably determined.

We are unaware of work using EXAFS or XANES in which such systems containing quantum dots with magnetic impurities were studied, because in this case one has to investigate a thin (1–5 nm) surface layer with a small (a few percent) content of magnetic impurity.

In several studies [4, 5, 16–18] of structures obtained under similar conditions of growth (germanium quantum dots doped with manganese impurities obtained in a single epitaxy process), the direct interaction of Ge and Mn atoms was not characterized and microstructure parameters (interatomic distances and coordination numbers for Ge–Mn) were not determined. In samples of this sort, the number of manganese atoms that are in direct contact with germanium atoms is very small and probably insufficient for obtaining reliable information. Only Gunnella et al. [19] who carried out the synthesis of multilayer GeMn samples with a thickness of 40 nm by two methods (with sequential and simultaneous epitaxial deposition of Ge and Mn layers in the absence of silicon layers and without quantum dots) detected the direct interaction of Ge and Mn atoms was detected and Ge–Mn distances by the analysis of EXAFS Mn*K* spectra. According to their work, it is most likely that the manganese atoms at its low concentrations (of about 10%) are located in the sites of the Ge crystal lattice, as well as in the interstices of the Ge cubic lattice with coordinates (1/4; 1/4; 3/4) with a tetrahedral environment. The position of Mn atoms in the interstices of the Ge lattice with coordinates (3/8; 5/8; 3/8) with a hexagonal environment is unlikely according to [19]. In this work, we use the results of model calculations of experimental Mn*K* EXAFS spectra for MnGe clusters to determine interatomic distances in the nearest neighborhood of Mn. The two most probable positions of manganese atoms are: (1) the substitution for the Ge atom: the closest Mn_1–Ge distance is 2.44 Å; (2) the interstitial position in the tetrahedral environment: the Mn_2–Ge distances of 2.44 and 2.82 Å.

At higher concentrations, manganese can form a noticeable amount of structural phases with germanium (Ge_3Mn_5 ($T_C \approx 296$ K), Ge_8Mn_{11} ($T_C \approx 270$ K) [16, 19]) or agglomerate into metal clusters [16] in the form of nanowires or nanoscale filaments [5]. However, it should be noted that, according to [5], at manganese concentrations of up to 10%, up to 75% of Mn atoms are found in germanium quantum dots, and at concentrations above 10%, manganese atoms diffuse into the strained overlaying covering silicon layer and into the strained (stretched in the plane of growth) layer of silicon under the quantum dots of germanium.

2. SYNTHESIS OF STRUCTURES

Structures with SiGe quantum dots with different Mn contents were grown in a molecular beam epitaxy (MBE) setup equipped with an electron beam evaporator for Si and crucibles for Mn and Ge. After the standard chemical cleaning procedure, the Si(100) substrates were loaded into the chamber of the MBE setup. Then, the surface of the loaded samples was cleaned by removing the protective layer of SiO_2 at a temperature of 750°C in a weak flow of Si. To avoid the undesirable influence of possible residual surface contamination on the formation of structures, for all the samples, a buffer layer of silicon, 100 nm thick, was deposited at a temperature of 500°C on a clean substrate surface. Germanium layers were deposited on substrates with a grown Si buffer layer with simultaneous Ge and Mn flow: manganese at different substrate temperatures in the range from 400 to 550°C. The rate of Ge deposition was about 0.1 Å/s. The amount of

deposited Ge was 7.5 monolayers (ML) in samples 32–35 and 8 ML in samples 44–48, and the amount of manganese varied from one sample to another by changing the rate of Mn deposition.

Figure 1 shows the diagrams of the synthesized structures. The concentration of Mn in the samples depends on the synthesis temperature and the Mn deposition rate during the synthesis, which are given in Table 1. The values of the percentage of Mn, obtained from Rutherford backscattering experiments, for samples 32, 33, 34, and 35 are approximately 22, 8, 4, and 11%, respectively. Under the indicated conditions of synthesis, the joint deposition of Ge and Mn on the silicon surface led to the formation of three-dimensional GeMn nanoislands (quantum dots). According to the data obtained by atomic force microscopy (AFM), an increase in the manganese content in the studied structures leads to an increase in the size of quantum dots and a decrease in their density (Fig. 2a). It follows from the AFM data that manganese plays the role of a surfactant, whose presence on the surface of the growing film leads to an increase in the surface diffusion coefficient and to the enlargement of the islands and a decrease in their density. The effect is similar to an increase in the growth temperature. At high concentrations of manganese (higher than 20%), a catalytic effect manifests itself: manganese accumulates on one side of the island and stimulates growth in this direction, leading to the formation of nanowires on the surface of structures (Fig. 2b).

In all samples, the layer of quantum dots GeMn was covered by a silicon layer with a thickness of about 20 nm. When quantum dots are covered with silicon, the Ge/Si interface can loosen. Therefore, in samples 32–35 of the first series, quantum dots were covered with a thin (2 nm) protective silicon layer at a temperature of 200°C, after deposition of which a high temperature 400°C silicon layer 20 nm thick was deposited. In samples 44–48 of the second series, the low-temperature layer was absent.

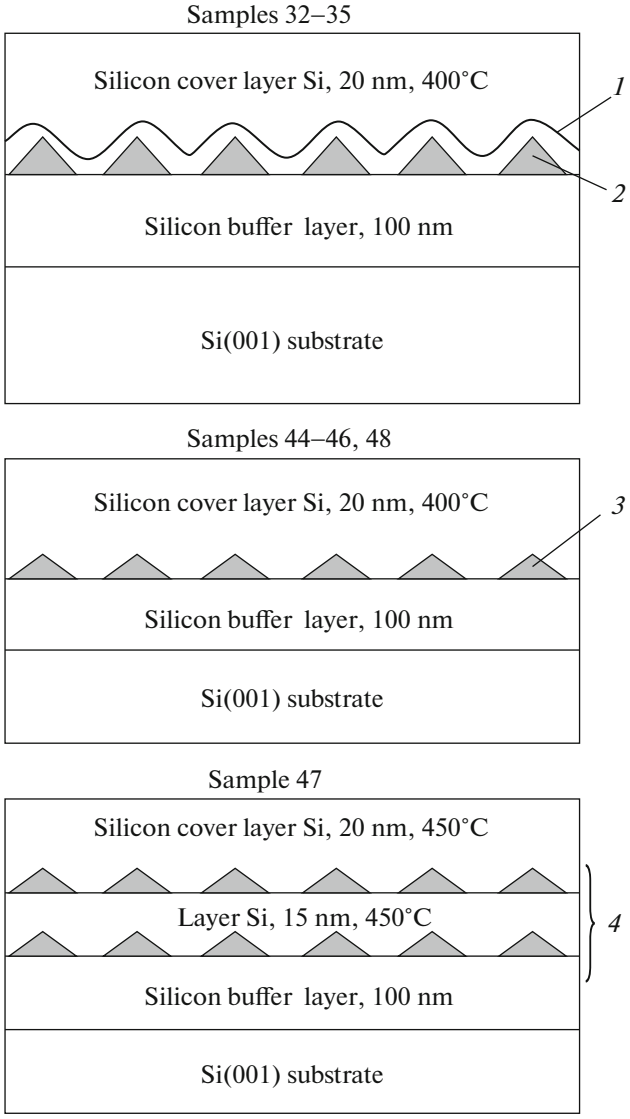

Fig. 1. Schemes of Si/GeMn samples obtained by MBE under different conditions and with different contents of manganese impurity: (*1*) low-temperature (200°C) silicon layer, 2 nm; (*2*) MnGe quantum dots, 7.5 ML Ge; (*3*) MnGe quantum dots, 8 ML Ge; (*4*) five double layers of MnGe quantum dots separated by a silicon layer; 8 ML Ge; *T*, °C is the synthesis temperature; effective thicknesses are in monolayers of quantum dots.

3. EXPERIMENT AND SIMULATION

3.1. XAFS Spectra Recording

XANES and EXAFS spectra were recorded using a Rossendorf Beamline (ESRF, Grenoble, France) in the fluorescent mode at room temperature. Si(111) was used as an input monochromator crystal; two mirrors with Rh coating were used to focus the beam in the horizontal and vertical planes. Fluorescent radiation from the samples was sensed by a twelve-element germanium detector. The flux of quanta in the germanium spectra of was about 3×10^{11} photon/s in a 200 μm × 5 mm beam. Plates with semiconductor structures were glued to the table and placed under a beam of monochromatic synchrotron radiation at an angle of about 1°. EXAFS spectra were measured at the Ge*K* absorption edge in the energy range 10858–12082 eV, which corresponds to the wavenumber range k of up to 14 Å^{-1} (the Ge*K* energy absorption edge is 11103 eV). For some samples with a high manganese content, we managed to record the XANES spectra in the *K*-edge region of manganese absorption. The oscillating parts of the absorption spectra $\chi(k)$ in the range $\Delta k = 3$–13 Å^{-1} and the Fourier-transform modules (radial structure functions without phase shift) of experimental Ge*K*-spectra of EXAFS samples 32–35 (Fig. 3) with a protective low-temperature silicon coating) and samples 44–48 (without silicon coating) (Fig. 4) were obtained using the VIPER program [20]. EXAFS

Table 1. Modeling of germanium spectra taking into account manganese (second model)

Sample	Growth conditions		N(Ge) (±0.1)	N(Si)	$N(Mn_1) + N(Mn_2)$	$R(Mn_1; Mn_2)$, Å	$N(Mn_2)$	$R(Mn_2)$, Å	$2\sigma^2$, Å^2 (±0.001)	F
	T(Ge), °C	Mn evaporation rate, Å/s								
32	450	0.02	1.8	2.1	0.9 ± 0.2	2.49 ± 0.01	0.5 ± 0.1	2.85 ± 0.01	0.012	1.6
33	450	0.01	1.9	2.1	0.3 ± 0.1	2.45 ± 0.01	0.2 ± 0.1	2.82 ± 0.02	0.010	1.5
34	450	0.005	2.0	2.0	0.2 ± 0.1	2.44 ± 0.03	0.3 ± 0.1	2.85 ± 0.02	0.011	1.6
35	550	0.01	1.7	2.3	0.4 ± 0.2	2.60 ± 0.03	0.2 ± 0.2	2.86 ± 0.02	0.011	1.5
44	500	0.005	1.6	2.3	–	–	0.3 ± 0.2	2.86 ± 0.03	0.010	1.4
46	400	0.005	2.1	1.9	0.1 ± 0.1	2.43 ± 0.03	0.2 ± 0.1	2.80 ± 0.02	0.010	1.1
47	450	0.005	1.7	2.3	–	–	0.3 ± 0.2	2.81 ± 0.01	0.010	1.2
48	450	0.005	1.9	2.1	–	–	0.2 ± 0.1	2.87 ± 0.01	0.011	0.6
45	450	0.005	1.1	2.9	–	–	–	–	0.008	1.5

Initial conditions for calculation: model (Ge)–(Ge, Si, Mn_1, Mn_2); N_1(Ge) + N_2(Si) = 4. All Debye factors are equalized: $\sigma_1^2 = \sigma_2^2 = \sigma_3^2 = \sigma_4^2 = \sigma^2$; ΔR = 1–2.7 Å, Δk = 3–13 Å^{-1}; R(Ge–Ge) = 2.44 Å, R(Ge–Si) = 2.39 Å; $N(Mn_1)$ are the coordination numbers for manganese atoms located at the sites of the germanium cubic lattice (substitution); $N(Mn_2)$ are the coordination numbers for manganese atoms located in interstices with a tetrahedral environment (interstitial dissolution); F is the fitting factor characterizing the divergence of the experimental and fitted spectra.

spectra were simulated using the software package EXCURVE 98 [21].

3.2. Processing and Simulation of EXAFS Spectra

The microstructure parameters of the GeMn/Si quantum dots were determined from an analysis of experimental Ge*K* (rather than Mn*K* as in [19]) EXAFS spectra, since the samples under study contain a very small number of manganese atoms (several atomic percents of several deposited GeMn/Si monolayers), and much more germanium atoms, and the spectra of germanium are much more intense than the spectra of manganese.

We propose simple EXAFS simulation schemes that include only the nearest-neighbors of the absorbing atom (ΔR = 1.0–2.8 Å) and a small number of structural parameters to be determined, which can help find and quantitatively characterize the presence of manganese in the immediate vicinity of germanium atoms. In the framework of such schemes, the original

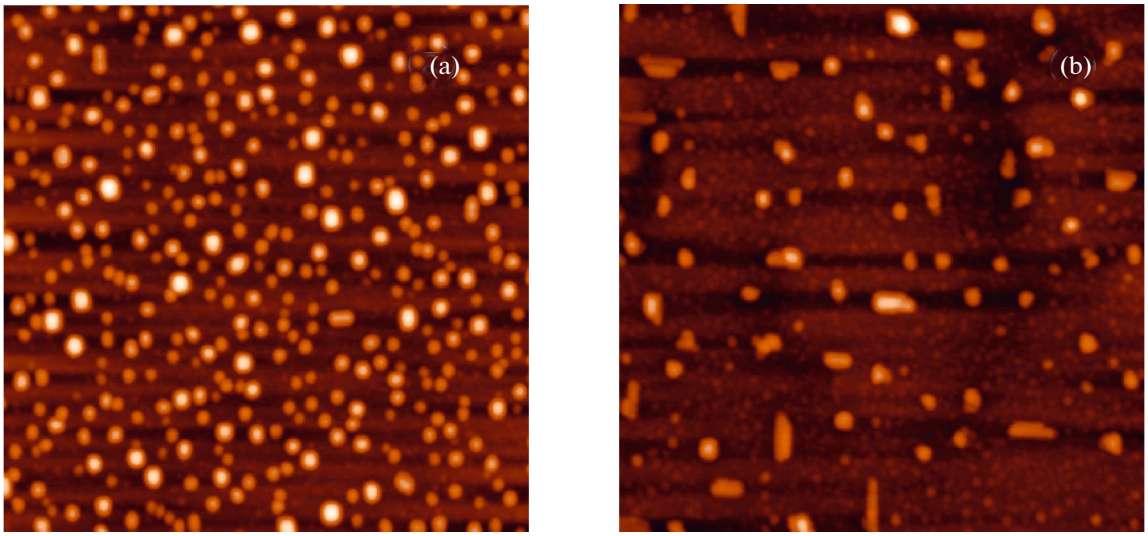

Fig. 2. (Color online) AFM images (1.5 × 1.5 μm^2) of the surface structures of the $Mn_{1-x}Ge_x$/Si(100) obtained by germanium deposition (7.5 ML) with different ratios of Mn/Ge: (a) 4%; (b) 21%. Germanium and manganese deposition temperature is 450°C. The rate of germanium deposition is 0.1 Å/s.

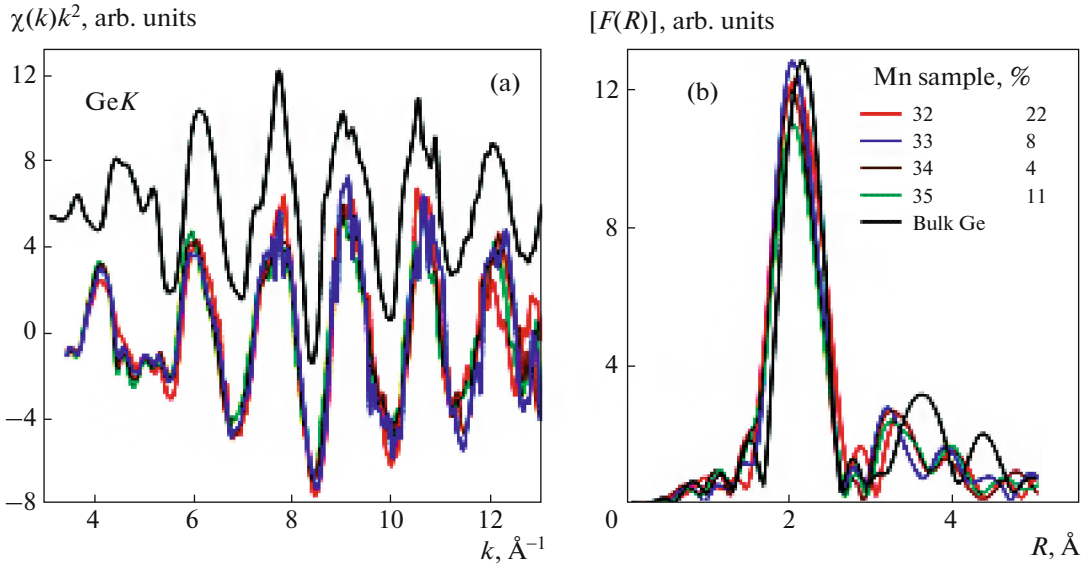

Fig. 3. (Color online) (a) Experimental Ge*K* EXAFS spectra of samples 32–35 with different Mn content, determined by the Rutherford backscattering method, and with a low-temperature (200°C) protective layer, 2 nm thick. (b) Fourier-transform modules (radial structure functions without taking into account a phase shift) of experimental Ge*K* EXAFS spectra of samples 32–35.

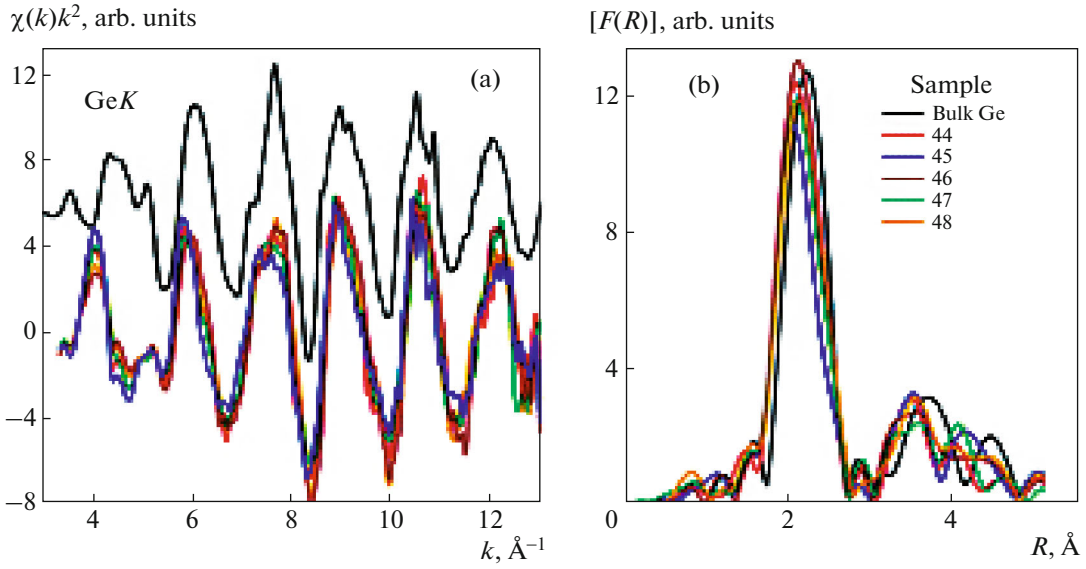

Fig. 4. (Color online) (a) Experimental Ge*K* EXAFS spectra of samples 44–48 without low-temperature protective coating of silicon and with different growth temperatures of quantum dots. (b) Fourier-transform modules (radial structure functions without taking into account a phase shift) of experimental Ge*K* EXAFS spectra of samples 44–48.

spectra were "filtered" with respect to *R* and the contribution from scattering on nearest neighbors of germanium atoms was selected.

Analysis of literature data [19] suggests that manganese atoms are in several possible structural states in the system under study: (1) in the sites; (2) in the interstices of the germanium matrix diluted with silicon; (3) in stoichiometric phases with germanium; (4) in metal clusters. At the preliminary stage of calculation the Ge–Ge, Ge–Si, and Ge–Mn coordination numbers were varied ("released"), and as a result, it was found that their sum is very close to four.

In the first approximation (for the calculation of Ge–Ge and Ge–Si interatomic distances), the spectra were simulated without taking into account manganese atoms. The simulation results give distances Ge–Ge = 2.44 Å and Ge–Si = 2.39 Å, which are in good agreement with our data obtained earlier in the

analysis of structures with germanium quantum dots [14, 15]. These distances were then taken constant in the calculation of structures taking into account manganese atoms.

In accordance with [19], it was suggested that, in the simultaneous epitaxy of germanium and manganese, manganese atoms substitute for germanium atoms (and in the case of quantum dots, substitute for silicon atoms) or occupy positions with coordinates (1/4; 1/4; 3/4) in the interstices of germanium cubic lattice with a higher probability.

3.3. Two Variants of the Structural Model

When simulating the spectra of our Si/GeMn samples with quantum dots, we included in the consideration: (1) only one starting distance Ge–Mn = 2.44 Å for the first model with the substitution of manganese atoms for germanium or silicon; (2) substitution (starting distance Ge–Mn = 2.44 Å) and incorporation into interstices (starting distances Ge–Mn = 2.44 Å, 2.82 Å) in accordance with [19] for the second model that includes both variants of manganese positions in the lattice. All the indicated distances correspond to the first scattering maximum (see Figs. 3b and 4b), which we considered in the simulation after "filtering" in the *R*-space of experimental spectra.

To eliminate possible errors in the "fitting" of a large number of parameters, the reference spectrum of the pure germanium film (50 Å thick) was calculated and the following parameters were obtained for it: $S_0^2 = 0.89$ is the factor of amplitude suppression due to many-electron processes and $E_F = -13.1$ eV is the "Fermi level energy." These parameters were then fixed in the calculations of other spectra.

3.4. The First Variant of the Model

Manganese atoms substitute for germanium atoms in a cubic lattice; the total coordination number of Ge atoms is Ge + Si + Mn = 4; the initial Ge–Mn distance in the simulation is the same as a Ge–Ge distance of 2.44 Å. The first variant of the model can be used when manganese atoms substitute for germanium (or silicon) atoms in the lattice sites or are at close distances from germanium atoms. As a result of processing and selecting the most appropriate model to describe the experimental data, it was found that the obtained values of coordination numbers and distances do not fit well the data obtained by other methods, and their changes do not correspond to changes in the conditions of synthesis. Therefore, the variant of the structure of the system, in which only the substitution of manganese atoms for germanium and silicon atoms in the lattice and the absence of manganese atoms in the interstices is apparently wrong. Since, in our case, this is not the only possible arrangement of manganese atoms, a second variant of the model is proposed: manganese both in the sites and in the interstices in accordance with [19].

3.5. The Second Variant of the Model

Taking into account that most of the germanium atoms are inside the tetrahedra consisting of germanium and silicon atoms, and fewer are inside the tetrahedra including also a manganese atom, the atomic environment of germanium in all cases is set by the sum Ge + Si = 4, and the manganese atoms are taken into account in two positions in addition to four Ge + Si atoms. Initially, manganese atoms were placed at a distance of 2.44 Å (in the lattice sites) and 2.44 and 2.82 Å (in the interstices), in accordance with our assumptions based on the results of [19], and then they were refined (they were "released") in the simulation process.

The data obtained for the second model are presented in Table 1.

4. RESULTS AND DISCUSSION

According to the results obtained in the second variant of the structural model, for the coordination numbers of manganese atoms relative to germanium atoms, a good agreement was found with the technological conditions of synthesis, that is, for example, there was a correlation between the amount of manganese in the samples and the rate of its evaporation (see Table 1).

As can be seen from the table, we were unable to obtain for the second model complete sets of microstructural data related to the manganese atoms for a part of the samples with a low concentration of manganese. The accuracy of our experiment did not allow us to obtain reliable microstructural data for these samples in this a model. This is likely due to the fact that in samples 44–48 without a protective low-temperature silicon layer over the germanium quantum dots, the manganese concentration is somewhat lower, because during the synthesis process manganese diffusion occurred not only into the strained less dense silicon layer under the quantum dots, but also in the covering layer of silicon. It can be noted that for sample 46, obtained at the lowest temperature (400°C), the coordination number of manganese was nevertheless determined, but its value (0.1 ± 0.1) is at the level of determination error and corresponds to a manganese concentration of about 2% Samples 45 and 35 were obtained at the highest temperature (550°C) and significant diffusion mixing (coordination numbers N(Ge–Ge) = 1.1 and N(Ge–Si) = 2.9 for sample 45 without protective layer and N(Ge–Ge) = 1.7 and N(Ge–Si) = 2.3 for sample 35 with a protective low-temperature silicon layer). Therefore, complete structural characterization of manganese atoms proved to be impossible for these samples.

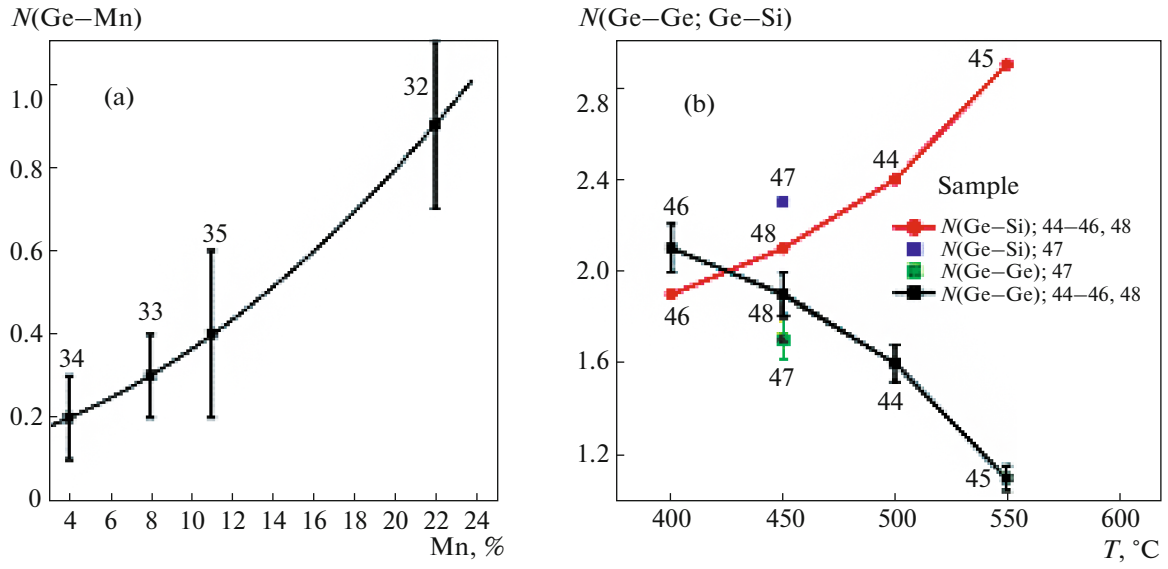

Fig. 5. (Color online) (a) Correlation of concentration dependences for manganese in Si/GeMn quantum dots for samples 32–35. The manganese content was determined by the RBS method (Mn concentration in percent, abscissa axis) and using EXAFS measurements (N(Ge–Mn) average coordination numbers, ordinate axis). (b) The dependence of the average coordination numbers N(Ge–Ge) and N(Ge–Si) on the temperature of sample synthesis.

For the second model, the atomic Mn/Ge ratio was estimated taking into account the manganese atoms that are located in the nearest neighborhood of germanium atoms and substitute for germanium atoms in the structure (R(Ge–Mn) ≈ 2.44 Å) or are in the interstices of the lattice with tetrahedral coordination (R_1(Ge–Mn) ≈ 2.44 Å, R_2(Ge–Mn) ≈ 2.82 Å) [19]. The ratio

$$\text{Mn/Ge} = ([N(\text{Mn}_1) + N(\text{Mn}_2)]/[4(\text{neighboring atoms}) + 1(\text{abs. atom})]) \times 100\%$$

is 18% for sample 32, 16% for sample 33, 4% for sample 34, and 8% for sample 35. Thus, the Mn/Ge percent ratio determined from our data for the studied samples are not too different from those obtained from Rutherford backscattering (22% for sample 32, 8% for sample 33, 4% for sample 34, and 11% for sample 35) and correspond to changes in the conditions of synthesis (see Table 1). For samples 44–48, the estimated Mn/Ge atomic percent ratio is 2–6% or less (given the accuracy of our measurements and simulations).

Both variants of the model are approximate but give very close values for the coordination numbers germanium and silicon with respect to germanium for and for all interatomic distances. It should be emphasized that intensive mixing of germanium and silicon atoms (comparable contents of germanium and silicon in quantum dots) was found in both models for all samples. The degree of diffusion correlates with the growth temperature of quantum dots and the evaporation rate (concentration) of manganese. Thus, a good agreement of the microstructural parameters with the growth conditions has been found for the second model, which takes into account manganese located both in the lattice sites and in the interstices. It may be noted here that the coordination numbers for Mn_1 + Mn_2 are noticeably higher than for Mn_2 in sample 32 with a high concentration of manganese (about 20%) and somewhat higher most of other samples (see Table 1). This effect can be explained by the presence of manganese both in the sites and in the interstices, because in the first case (for Mn_1 + Mn_2) the contribution to the coordination numbers corresponds to the sites and interstices, and in the second (for Mn_2), only to the interstices. Thus, our results suggest the presence of manganese with tetrahedral coordination in interstices, as well as the substitution of manganese for germanium at the lattice sites.

Figure 5a shows the correlation of concentration dependences for the manganese content in samples with Si/GeMn quantum dots determined by Rutherford backscattering (horizontal coordinate) and coordination numbers determined by EXAFS measurements (vertical coordinate).

Figure 5b shows the dependence of the average coordination numbers N(Ge–Ge) and N(Ge– Si) on the synthesis temperature of the samples. The dependence is almost linear, with the exception of multilayer sample 47, for which the diffusion is much more significant because of its repeated (ten-fold) heating in the process of synthesizing layers of quantum dots.

In the simulation, within the framework of the adopted procedure of EXAFS processing for the studied samples metallic manganese, the Ge_3Mn_5 phase, which is most often formed during the epitaxy of man-

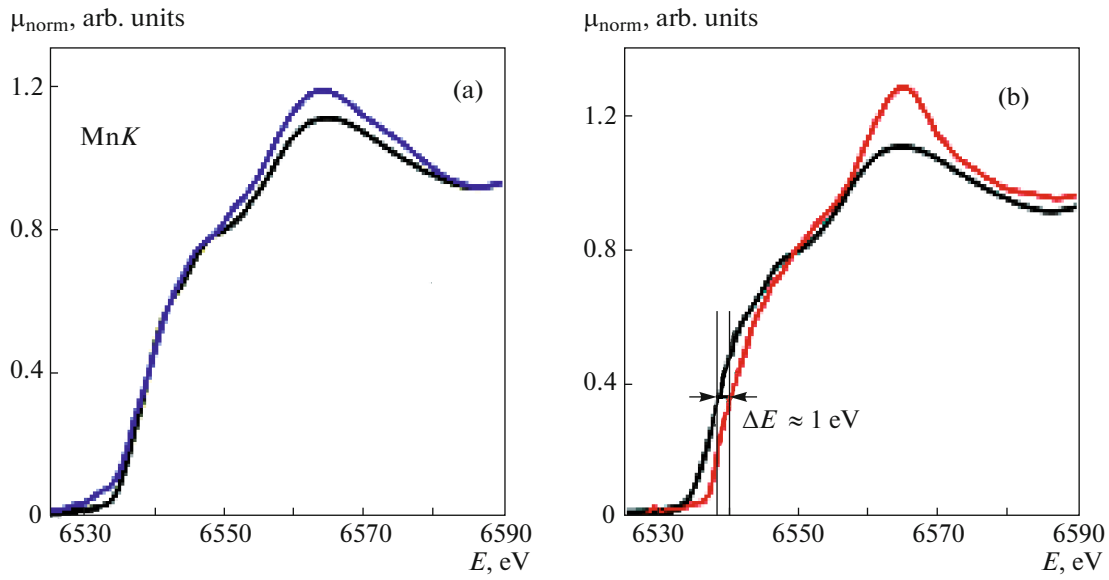

Fig. 6. (Color online) (a) Mn*K* absorption edges of the reference sample of Mn foil (black curve) and sample 32 with quantum dots (blue curve). (b) Mn*K* absorption edges of the reference sample of Mn foil (black curve) and sample with GeMn quantum dots obtained by ion implantation of Mn^+ (red curve).

ganese and germanium in the absence of silicon, and the Ge_8Mn_{11} phase were not detected in a significant amount in any of the samples.

Figure 6a shows the Mn*K* XANES spectrum, which was obtained only for the sample with the highest concentration of manganese (18% according to our data and 22% according to Rutherford backscattering); for other samples, we failed to obtain reliable data. The Mn*K* spectrum for sample 32 is close in shape and position of the absorption edge to that of the metallic manganese.

For comparison, Fig. 6b shows the Mn*K* XANES spectrum, which was recorded for the sample obtained by Mn^+ ion implantation. The shift of the Mn*K* absorption edge for a sample irradiated by ions is about 1 eV and corresponds to the presence of a certain amount (on the order of a few percent) of positively charged manganese.

5. CONCLUSIONS

The discovery and study of FM semiconductors may make it possible to realize the potential advantages of new functional elements from materials that dissipate low power. Si/GeMn structures containing layers of spatially ordered quantum dots are very promising in this sense. For systems of this sort, the FM behavior at rather high temperatures (above 400 K) is studied. Samples with different topologies and magnetic impurity contents were synthesized for our study using the MBE Si/GeMn method.

For the first time, using extended X-ray absorption fine structure (EXAFS) and X-ray absorption near edge structure (XANES) spectroscopy, atomic force microscopy, Rutherford backscattering, we studied the features of the microstructure and elemental composition of Si/GeMn magnetic systems obtained by MBE and containing quantum dots.

Coordination numbers and interatomic distances are determined from the analysis of Ge*K* EXAFS spectra. Intensive mixing of germanium and silicon atoms was found in all samples and the degrees of Ge, Si, Mn atom diffusion was found to correlate with the synthesis conditions of samples with Si/GeMn quantum dots.

For these systems, direct contacts of germanium atoms with manganese atoms are characterized and the presence of interstitial manganese with tetrahedral coordination and substitution of manganese for germanium and silicon in the lattice sites, was found. Stoichiometric phases Ge_8Mn_{11} and Ge_3Mn_5 were not detected.

The correlations of the Ge, Si, and Mn coordination numbers in the germanium environment are determined with both the Mn flux value (evaporator temperature) and with the temperature at which quantum dots are grown, as well as with other conditions of synthesis. The manganese concentration in the samples is determined.

ACKNOWLEDGMENTS

This work was supported in part by the Russian Foundation for Basic Research (grant nos. 16-02-00175_a (XAFS spectroscopy study), 16-02-00397_a (Synthesis of structures)).

REFERENCES

1. G. Busch, P. Junod, and P. Wachter, Phys. Lett. **12**, 11 (1964).
2. I. I. Lyapilin and I. M. Tsidil'kovskii, Sov. Phys. Usp. **28**, 349 (1985).
3. S. G. Ovchinnikov, Phase Trans. **36**, 15 (1991).
4. F. Xiu, Y. Wang, J. Kim, A. Hong, J. Tang, A. P. Jacob, J. Zou, and K. L. Wang, Nat. Mater. **9**, 337 (2010).
5. J. Kassim, C. Nolph, M. Jamet, P. Reinke, and J. Floro, J. Appl. Phys. **113**, 073910 (2013).
6. X-ray Absorption: Principles, Applications, Techniques of EXAFS, SEXAFS, and XANES, Ed. by D. C. Koninsberger and R. Prins (Wiley, New York, 1988).
7. D. I. Kochubei, Yu. A. Babanov, K. I. Zamaraev, L. N. Mazalov, et al., *X-Ray Spectral Method for Studying the Structure of Amorphous Bodies: EHAPS Spectroscopy* (Nauka, Novosibirsk, 1988) [in Russian].
8. A. V. Kolobov, H. Oyanagi, K. Brunner, and K. Tanaka, Appl. Phys. Lett. **78**, 451 (2001).
9. A. V. Kolobov, H. Oyanagi, Sh. Wei, K. Brunner, G. Abstreiter, and K. Tanaka, Phys. Rev. B **66**, 075319 (2002).
10. A. V. Kolobov, H. Oyanagi, A. Frenkel, I. Robinson, J. Cross, Sh. Wei, K. Brunner, G. Abstreiter, Y. Maeda, A. Shklyaev, M. Ichikawa, S. Yamasaki, and K. Tanaka, Nucl. Instrum. Methods Phys. Res., Sect. B **199**, 174 (2003).
11. F. Boscherini, G. Capellini, L. di Gaspare, F. Rosei, N. Motta, and S. Mobilio, Appl. Phys. Lett. **76**, 682 (2000).
12. A. Karatutlu, W. R. Little, A. V. Sapelkin, A. Dent, F. Mosselmans, G. Cibin, and R. Taylor, J. Phys.: Conf. Ser. **430**, 012026 (2013).
13. Yu. Zhang, O. Ersoy, A. Karatutlu, W. Little, and A. Sapelkin, J. Synchrotr. Rad. **23**, 253 (2016).
14. S. Erenburg, N. Bausk, L. Mazalov, A. Nikiforov, and A. Yakimov, J. Synchrotr. Rad. **10**, 380 (2003).
15. S. B. Erenburg, N. V. Bausk, L. N. Mazalov, A. I. Nikiforov, and A. I. Yakimov, Phys. Scr. **115**, 439 (2005).
16. T. Nie, X. Kou, J. Tang, Y. Fan, S. Lee, Q. He, Li-Te Cgang, K. Murata, Y. Gen, and K. L. Wang, Nanoscale **9**, 3086 (2017).
17. M. Aouassa, I. Jadi, A. Bandyopadhyay, S. K. Kim, I. Karaman, and J. Y. Lee, Appl. Surf. Sci. **397**, 40 (2017).
18. I. T. Yoon, C. J. Park, S. W. Lee, T. W. Kang, D. W. Koh, and D. J. Fu, Solid State Electron. **52**, 871 (2008).
19. R. Gunnella, N. Pinto, L. Morresi, M. Abbas, and A. di Cicco, J. Non-Cryst. Sol. **354**, 4193 (2008).
20. K. V. Klementiev, VIPER for Windows, freeware.
21. N. Binsted, EXCURV 98: CCLRC Daresbury Laboratory Computer Program (1998).

Translated by A. Zeigarnik